RESEARCH ARTICLE

ROLES OF THE QUADRUPOLE INTERACTION AND OF THE QUADRATIC STARK EFFECT IN SPECTRAL LINES FROM PLASMAS INTERACTING WITH A STRONG QUASIMONOCHROMATIC ELECTRIC FIELD

P. SAUVAN

Departamento de Ingeniería Energética, ETS Ingenieros Industriales, UNED, C/Juan del Rosal 12,28040 Madrid, Spain.

E. DALIMIER AND C. RICONDA

Laboratoire pour l'Utilisation des Lasers Intenses UMR 7605, CNRS-CEA-Ecole Polytechnique-Université Paris 6, case 128, 4 Place Jussieu, 75252 Paris Cedex 05 and 91128 Palaiseau, France.

E. OKS

Physics Department, 206 Allison Laboratory, Auburn University, Auburn, AL 36849, USA.

O. RENNER

Institute of Physics, Academy of Sciences CR, Na Slovance 2, 18221 Prague, Czech Republic.

S. WEBER

CELIA Université Bordeaux-CNRS-CEA, 33405 Talence, France.

Abstract: We present an advanced analysis of the spectroscopic signatures of the interaction of a strong Quasi-monochromatic Electric Field (QEF), generated by a high-power short-pulse laser, with a preformed laser-produced plasma. The computation of a synthetic spectrum emitted by such plasmas requires the calculation of the Stark line shape in the presence of a QEF and the evaluation of the QEF intensity profile throughout the line of sight in the plasma. Stark profiles in hot dense plasmas containing a strong QEF are calculated using the so-called Floquet-Liouville formalism. In this paper, in distinction to our previous publications, we studied the roles of the quadrupole interaction with the ion microfield and of the quadratic Stark effect. Then Particle-In-Cell (PIC) kinetic simulations were performed for taking into account the inhomogeneity of the QEF intensity. These theoretical calculations were applied for a spectroscopic analysis of the experimental Al He β line. The spectroscopic signatures of the QEF are prominent satellites, non-symmetrical with respect to the unperturbed line and distinguishable from the dielectronic satellites. We found that the allowance for the quadratic Stark effect was important for the consistent interpretation of the experimental results, while the allowance for the quadrupole interaction with the ion microfield did not play a significant role.

PACS: 52.38.-r, 32.70.-n, 52.70.-m, 32.60.+i.

1. INTRODUCTION

In a recent paper [1] we presented general principles of spectroscopic diagnostics of plasmas containing a Quasi-monochromatic Electric Field (QEF). We also provided an analysis of the corresponding experimental data via advanced simulations coupling a spectral line shape code based on the Floquet-Liouville formalism with a Particle-In-Cell (PIC) kinetic code providing a spatial distribution of the QEF in the plasma.

The experimental profiles have been obtained from spectroscopic diagnostics designed for dense hot plasmas generated with two high-power short-pulse laser beams. The first beam is used to create the plasma, and a delayed high-power short pulse laser crosses the preformed plasma, generating a strong oscillating QEF. It is well known that under specific conditions of the present experiment, the plasma does exist when the first laser is off [2]. The experiment and the spectroscopic diagnostics were performed at the Jena laser system JETI [3, 4]. The short-pulse laser interaction with the pre-formed plasma was described by a PIC kinetic simulation code yielding, in particular, the spatial distribution of the QEF in the plasma.

So, at the focus of paper [1] were effects of the external strong QEF — due to the second laser — on the Stark profiles. Some signatures of externally introduced laser fields in x-ray emission had been previously exhibited using the same experimental device [3, 4]. It is important to emphasize that, in those situations, no plasma waves (which might have been caused by the interaction of the pre-formed plasma with the first laser) are involved, since the first laser is off during the registration of the spectral line profiles at given distances from the target surface.

The analysis in paper [1] provided an overall satisfactory interpretation of the experimental data. However, some experimental features remained unexplained. For example, a tentative explanation of one of the features was through a hypothesis that it was a dipole-forbidden transition $1s^2 \, ^1S_0 – 1s3s \, ^1S_0$ activated by the coupling of the singlet states $^1S_0$ and $^1D_0$ via the quadrupole interaction with the ion microfield.

Therefore in the present paper we studied the role of the quadrupole interaction with the ion microfield. We also studied the role the quadratic Stark effect. The results are presented below.

2. EXPERIMENTAL SETUP AND THE FIELD-MODIFIED AL HE-BETA LINE

The experimental data needed for comparison with the theory were collected at the Jena multi-terawatt Ti:sapphire laser system JETI [5]. The laser routinely provides 1 J of energy, a pulse duration of 80 fs (FWHM), and repetition rate of 10 Hz. In the experiment, the laser pulse with the wavelength of 0.8 μm was stretched to 12.5 ps and the energy of 0.65 J delivered at the entrance window of the interaction chamber was split into two beams [4]. The near-target configuration of these beams, which were focused by off-axis parabolic mirrors to foci with a diameter of about 20 m, is schematically shown in Fig. 1. The plasma producing laser beam (0.2 J, 5×10^{15} W/cm²) was introduced to the chamber via a delay line and focused to a flat tip of the tapered Al target. The second beam (0.45 J, 1.2×10^{16} W/cm²) with the axis parallel to the target surface was hitting the plasma plume transversally. The axis of the plasma expansion, the electric field of the second beam and the direction of the x-ray spectra observation were mutually perpendicular. The electric field vector of the second laser beam was approximately perpendicular to the line of sight of the spectra, i.e. the transverse-field-affected line profiles were observed.
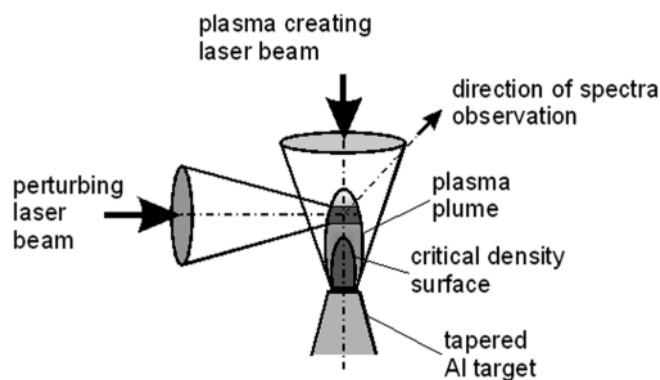

Fig. 1: Schematic diagram of laser beams and target geometry

Both focused laser beams were spatially overlapped and temporally synchronized with precision better than 1 ps. The timing and positioning of the perturbing beam above the target surface with respect to the plasma critical density surface (for the laser wavelength of 0.8 μm, this corresponds to the electron density $n_c = 1.7 \times 10^{21}$ cm⁻³) and the duration of the Al Heβ emission were optimized using predictions of one-dimensional plasma simulations [4]. The conclusions following from this modeling can be recapitulated in two points. Even at a short distance of 20 μm above the target, the Al Heβ emission starts safely after termination of the plasma-creating beam that precludes direct field effects of this beam on the observed line emission. In contrast, a good temporal overlap of the plasma Al Heβ emission with the 50-ps-delayed perturbing beam is favorable for observation of field effects in the spectral line profiles. The macroscopic plasma parameters simulated in more detail by two-dimensional Lagrangian hydro-code CHIC [6] indicate that at the distance of 20 μm from the target, the quasi-flat distributions of the electron density Ne (well below the $n_c/4$) and temperature Te (slightly above 120 eV) exist with a transverse dimension comparable to the focal spot diameter. These parameters are well compatible with the desired laser field penetration into the preformed plasma and with the observation of the spectral line Al Heβ emission.

The x-ray spectra were measured with the toroïdally bent crystal spectrometer (TCS) using a crystal of quartz (10-1) with bending radii 150/106.4 mm and fitted with a CCD camera. The fulfillment of the focal condition for Al Heβ radiation [7] at the source-to-crystal distance of 83.8 mm resulted in a spectral resolution of 6100, a magnification of 1.77, and a spatial resolution of approximately 12 μm. The spectral range of 28 eV covered by the spectrometer was relatively small but sufficient to study the full profile of the Al Heβ emission centered at

1867.7 eV. Benefiting from the extremely high collection efficiency of the TCS, the spectra were recorded in single laser shots. Further details concerning the experimental configuration and the spectra calibration can be found in [4].

The unperturbed Al Heβ emission was observable up to a distance of about 90 μm above the target. The presence of the transverse laser beam introducing the external electric field into the plasma environment slightly increased the noise of the spectral records and, most importantly, induced distinct modulations into the line profiles. The field effects were varied by changing the time delay between both laser beams and the distance of the perturbing beam above the target. In agreement with simulations, the most pronounced spectra perturbations were observed with the transverse laser beam delayed by 50 ps and introduced at the distance of 20 μm above the target. The reproducibility of the perturbing-beam-induced structures in spectral profiles Al Heβ is
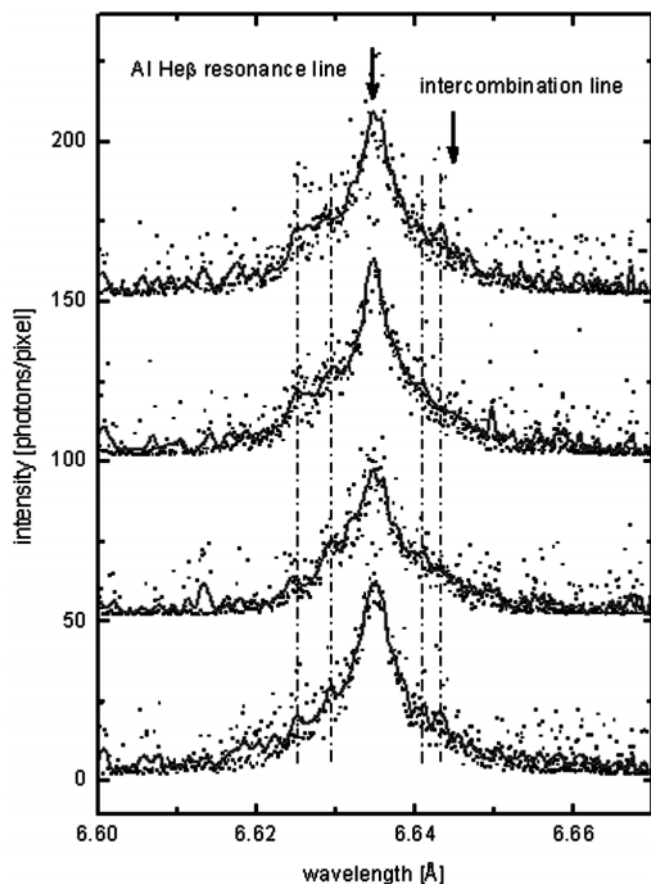

Fig. 2: Reproducibility of Al Heβ line profiles recorded in different shots. The experimental data (dots) are smoothed using the 5-point FFT (solid line). The bottom profile in this figure has been selected for comparison with theory and simulations.

demonstrated in Fig. 2, where the measured points are smoothed using the five-point fast Fourier transform. Albeit not all fine details are resolved in each spectrum, the presence of the dominant extremes in spectral line profiles is reasonably well reproducible. The identi-fication of these local maxima follows from detailed simulations presented in the next section.

3. GENERAL OVERVIEW OF THE SIMULATIONS

The Liouville space, usually employed to deal with the calculation of Stark profiles in dense plasmas, and the Floquet theory, developed to solve time periodic problems, have been joined together to solve the time-dependent Liouville equation in a so-called Floquet-Liouville formalism [8]. The Floquet-Liouville operator, introduced to solve the time-dependent problem (Stark effect in a time-dependent QEF), leads to a time-independent treatment carried out via an operator of the infinite dimension. Nevertheless, the periodic property of this operator allows one to consider only the projection of the Floquet-Liouville operator on the Floquet subspace of the fixed principal quantum number n. Depending on the coupling between the Floquet subspaces for the Floquet-Liouville operator, for any desired accuracy of the line shape calculation, there exists a value of n, at which the Floquet subspace can be truncated.

The effects of laser-plasma interaction relevant to the experiment performed at Jena are of two kinds. First, there is Raman and Brillouin back-scatterings, due to which the QEF amplitude in the plasma can be significantly higher than the amplitude of the second laser field in vacuum. Second, strong plasma oscillations are excited due to the parametric instability, resulting in the spatial modulation of the electron density.

The kinetic PIC simulations show that the spatial distribution of the electric field depends on the initial electron density profile in the plasma crossed by the second laser. Parabolic electron density profiles were introduced with different maximum densities.

The physical phenomena involved are sensitive to whether the maximum electron density is below or above one quarter of the critical density n_c. Above $n_c/4$, under the conditions of the present experiment, the dominant process is the stimulated Brillouin backscattering in the so-called strong coupling regime leading to the formation of transient phenomena, such as plasma cavities and transverse electromagnetic solitons [11].
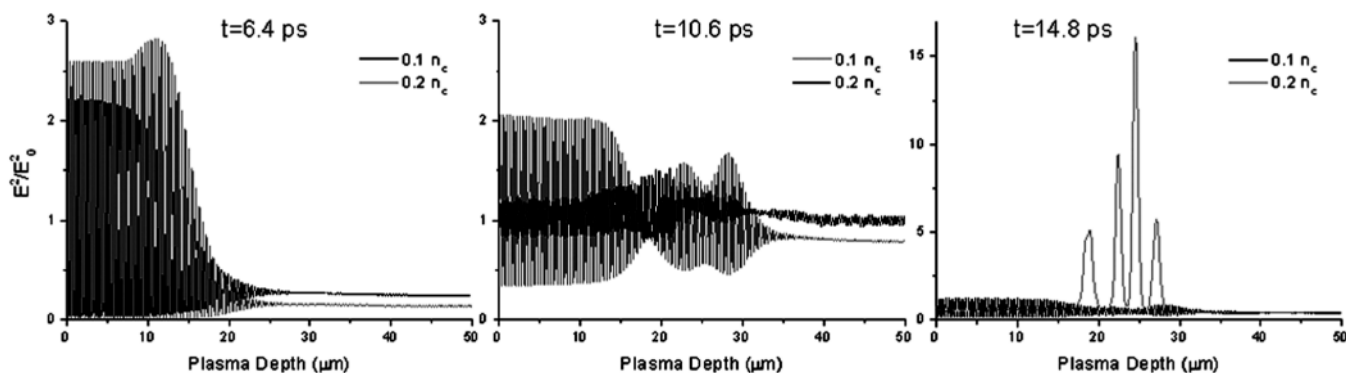
Fig. 3: Distribution of the energy density of the transverse QEF inside the plasma (the pulse is coming from the left) at three instants t. The values are normalized to the energy density of the incident laser field. For these PIC simulations, two average electron densities $0.1\,n_c$, $0.2\,n_c$ are considered and an average electronic temperature 150 eV has been chosen.

Figure 3 presents the results of the kinetic PIC simulations of the spatial distribution of the transverse time-averaged (over oscillating period) electric field in the plasma for initial electron densities $0.1\,n_c$ and $0.2\,n_c$ at three instants t during the second laser pulse. It shows significant changes compared to the laser field in vacuum and a strong dependence on the initial electron density.

4. SYNTHETIC FLOQUET-LIOUVILLE PROFILES

4.1 Space and Time Integrated Synthetic Profile

For a detailed comparison with the observed Al He spectra emitted from plasmas in the presence of QEF, we introduce synthetic line profile simulations obtained within the Floquet-Liouville formalism, and coupled with electric field PIC simulations.

The spectroscopic diagnostic has no time resolution. So we assume that the synthetic profile is a sum of two terms. The first term is due to the Al Heβ emission from the *perturbed plasma* existing only during the time interval T corresponding to the duration of the second laser pulse. The second term is due to the total Al Heβ emission of duration Δt_{unpert} from the *unperturbed plasma* before the second laser pulse. Both terms involve space integrations along the line of sight x and thus take into account the spatial transverse inhomogeneities.

Hence the synthetic profile is expressed as following:

$$\Phi_\nu \propto \int_0^T \left[1 - \exp\left(-\int_0^L k\left(\bar{N}_e, \bar{T}_e\right) \right) \varphi_\nu \left(E(x,t), \bar{N}_e, \bar{T}_e \right) dx \right] dt$$

$$+ \Delta T_{unpert} \left[1 - \exp\left(-\int_0^L k\left(N_e^0, T_e^0\right) \varphi_\nu^0 \left(N_e^0, T_e^0\right) dx \right) \right]$$

$$\dots (1)$$

In the *unperturbed profile* contribution, the normalized profile φ_ν^0 and the absorption coefficient k are calculated for a time/space average density N_e^0 characterizing the plasma before the second laser pulse. In the *perturbed profile* contribution, the normalized profile φ_ν and the absorption coefficient k are calculated for a time/space average density $\bar{N}_e$. This assumption is reasonable because the density affects the profiles weakly compared to the effect of the QEF. The average density is $\bar{N}_e$ smaller than N_e^0. This is because by the time, when the pulse of the second laser reaches its maximum, the plasma has already expanded transversally compared to its dimension during the emission of the "unperturbed profile".

So, the temporal and spatial dependences of the electric field are taken into account in the integrations in (1). These dependences are simulated by the PIC kinetic code. The profiles are calculated by the Floquet Liouville code including both the quadrupole interaction and the quadratic Stark effect.

4.2 Partial Profiles

In order to evaluate the space/time integrated synthetic profile, simulations for each set of parameters E, $\bar{N}_e$, $\bar{T}_e$ have to be done. For these simulations, only one value for $\bar{N}_e$ and one for $\bar{T}_e$ [1] have been considered, while only E is varying. Once those plasma parameters are set up, the atomic basis to be considered, i.e. the number of levels to include in the profile calculation, has to be fixed. Since the intensity of the QEF can be very high, the shifts due to the Stark interaction with this QEF can result in an overlapping of $n = 3$ and $n = 4$ levels (n is the principal quantum number). This effect is quite similar to the well-known high-density plasma effect when high n lines
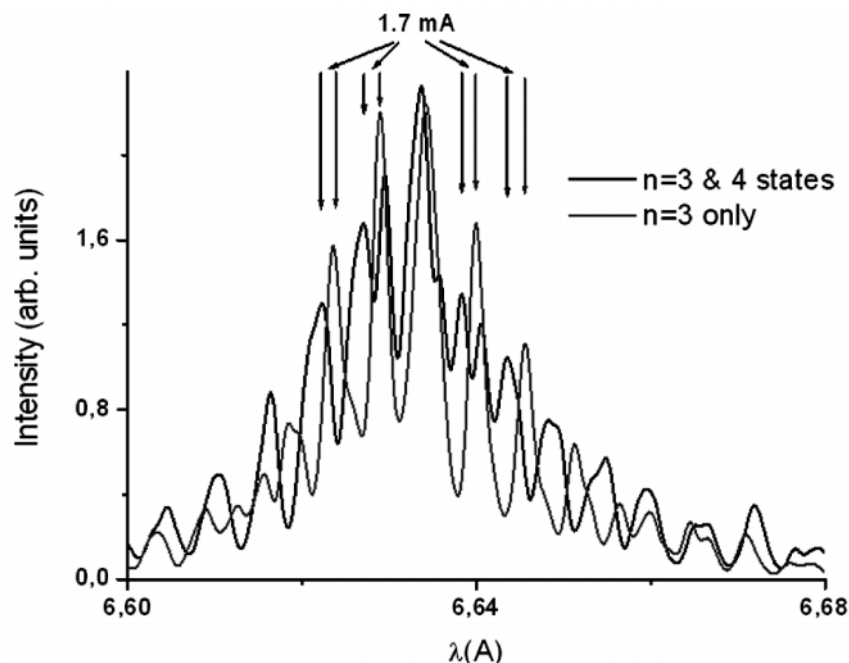
Fig. 4: Al Heβ profiles calculated considering either $n = 3$ states, or $n = 3$ and 4 states. The QEF intensity is $3\,\text{GV/cm}$.

overlap each other and merge in the continuum, due to the high values of the ionic microfield. In distinction, in the present study physically the root-mean-square value of the strong oscillatory electric field (rather than the quasistatic ionic microfield) is responsible for the overlapping of the multiplets $n = 3$ and $n = 4$. Figure 4 shows the effects of the choice of the atomic basis on the profile, considering only $n = 3$ states and considering $n = 3$ and $n = 4$ states in the Al-Heβ line calculation.

Two different spectral features can be exhibited in the comparison made in Fig. 4 between these two cases. The first one is a *shift* of the main line and its satellites when considering the enlarged atomic basis $n = 3$ and 4 states. This shift is about 1.7 mÅ, and it is in agreement with the quadratic Stark shift calculation as shown in [1]. The second feature is the *emergence of new satellites* due to the interaction of $n = 3$ and $n = 4$ states. This last feature was not exhibited in previous works [1] because the atomic basis used included only $n = 3$ levels.

This comparison concerns only the perturbed profile φ_v to be introduced in the synthetic profile.

4.3 Comparison Between Experimental and Synthetic Profiles

For all synthetic profiles, we chose an average

temperature $\bar{T}_e = 150$ eV, an optical depth $L = 50\ \mu\text{m}$, an average electron density $N_e^0 = 0.6\,n_c$, and the second laser pulse duration $T = 10$ ps (FWHM). The parameters $\bar{N}_e$ and Δt_{unpert} had to be fixed for the best agreement with the experimental results. Finally the synthesized profiles were convoluted with a Gaussian instrument function of 0.3 eV FWHM.

Figure 5 shows the full Al Heβ profile, simulated here for $\bar{N}_e = 0.2\ n_c = 3.3 \times 10^{20}\,\text{cm}^{-3}$ and $\Delta t_{unpert} = 8.9$ ps, and the comparison with the experimental profile. One of the main points in this final comparison is a good agreement for the intensity and the broadening of the central part of the Al Heβ line, as well as for the first two satellites in the blue side and for the first two satellites in the red side. More distant satellites in the simulated profile are located in the far wings, where the experi-mental profile merges into the noise.

This novel synthetic profile reproduces all the satellites located in the central part of the line — in distinction to our previous work [1]. Moreover, after allowing for the quadratic Stark effect via the enlarged atomic basis, there is no need to artificially shift the synthetic profile for the comparison with the experimental one. In work [1], the discrepancy concerning the second peak in the red wing of the line was tentatively attributed to a possible role of the quadrupole interaction with the ionic microfield, enhanced by the QEF.
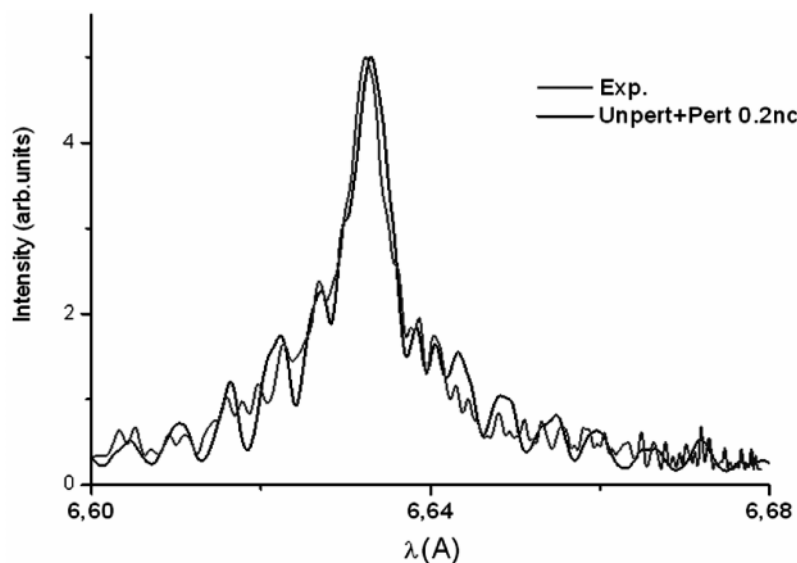
Fig. 5: Comparison between the simulated total ("perturbed" + "unperturbed") Al Heβ profile and the experimental profile. The parameters shown in the frame correspond to the best fit.

The authors of paper [12] had pointed out a *potential* importance of taking into account the quadrupole interaction for the interpretation of spectral line profiles in laser-produced plasmas. So, in our current simulations we have tested the *actual* importance of doing so.

Specifically, we tested the hypothesis from paper [1] that the unexplained experimental peak (the second one in the red wing) was a dipole-forbidden transition $1s^2\ {}^1S_0$ – $1s3s\ {}^1S_0$ activated due to the coupling of the singlet states ${}^1S_0$ and ${}^1D_0$ via the quadrupole interaction with the ion microfield. However, our current calculations of this effect showed that it was not strong enough to explain the experimental feature. It is the quadratic Stark effect introduced via the enlarged atomic basis that turned out to be important for the consistent interpretation.

5. CONCLUSIONS

We presented a complex analysis of the experimental Al He-beta emission from aluminum plasma created by one ps-laser beam and then subjected to another delayed ps-laser beam. The analysis was based on the advanced simulations coupling the code based on the Floquet-Liouville formalism with the kinetic PIC code that provides a spatial distribution of the QEF in the plasma. We demonstrated that the allowance for the quadratic Stark effect was important for the consistent interpretation of the experimental results, while the allowance for the quadrupole interaction with the ion microfield did not play a significant role.

REFERENCES

[1] P. Sauvan, E. Dalimier, E. Oks, O. Renner, S. Weber, C. Riconda, *J. Phys. B: At. Mol. Opt. Phys.*, **42**, 1950001, (2009).

[2] P. Audebert, R. Shepherd, K.B. Fournier, O. Peyrusse, D. Price, R.W. Lee, P. Springer, J.-C. Gauthier, and L. Klein, *Phys. Rev. Lett.*, **89**, 26500, (2002).

[3] O. Renner, P. Sauvan, E. Dalimier, C. Riconda, F.B. Rosmej, S. Weber, P. Nicolai, O. Peyrusse, I. Uschmann, S. Höfer, T. Kämpfer, R. Lötzsch, U. Zastrau, E. Förster, and E. Oks, in "Spectral Line Shapes", **19**, *AIP Conference Proceedings* 1058, 341, (2008).

[4] O. Renner, P. Sauvan, E. Dalimier, C. Riconda, F.B. Rosmej, S. Weber, P. Nicolai, O. Peyrusse, I. Uschmann, S. Höfer, R. Loetzsch, E. Förster, and E. Oks, "High Energy Density Physics", **5**, 139, (2009).

[5] Ch. Ziener, I. Uschmann, G. Stobrawa, Ch. Reich, P. Gibbon, T. Feurer, A. Morak, S. Düsterer, H. Schwoerer, E. Förster, and R. Sauerbrey, *Phys. Rev.*, **E 65**, 066411, (2002).

[6] J. Breil and P.-H. Maire, *J. Comput. Phys.*, **224**, 785 (2007).

[7] O. Renner, I. Uschmann, and E. Förster, *Laser Part. Beams*, **22**, 25, (2004).

[8] P. Sauvan and E. Dalimier, *Phys. Rev.*, **E 79**, 036405, (2009).

[9] A.C. Kolb and H. Griem, *Phys. Rev.*, **111**, 514, (1958).

[10] A. Calisti, F. Khelfaoui, R. Stamm, B. Talin, and R.W. Lee, *Phys. Rev.*, **A 42**, 5433, (1990).

[11] C. Riconda, S. Weber, V. Tikhonchuk, J.-C. Adam, and A. Heron, *Phys. Plasmas*, **13**, 083103, (2006). S. Weber, C. Riconda, V. Tikhonchuk, *Phys. Rev. Lett.*, **44**, 055005, (2005).

[12] V.P. Gavrilenko and Ya. O. Ispolatov, *Opt. Spectrosc. (USSR)*, **68**, 583, (1990).